JOURNAL OF THERMOPHYSICS AND HEAT TRANSFER
Vol. 9, No. 4, October–December 1995

Effect of Additives on the Regeneration of a Dilute Absorbent

Guoji S. Zheng* and William M. Worek†
University of Illinois at Chicago, Chicago, Illinois 60607-7022

Combined heat and mass transfer processes that occur when a liquid desiccant is regenerated in an open-cycle system have been investigated. The experimental setup consists of a channel where an absorbent solution flows over a heated plate and a stream of air flows over the liquid film in a counterflow arrangement. Additives were introduced to a liquid desiccant, a lithium chloride solution, and their effects on the transfer rates were studied using a two-wavelength fiber-optic holographic interferometer to determine the local heat and mass transfer coefficients from the air–liquid interface. The additives selected in this study were a surfactant, anionic sodium lauryl sulfate, and a polymer, anionic polyacrylamide.

Nomenclature

a_i = mass fraction of the ith component
b = fringe thickness
C_A = concentration of water vapor
C_A^* = dimensionless concentration of water vapor
D_{AB} = binary mass diffusion coefficient, m²/s
D_h = hydraulic diameter, m
$h_{m,x}$ = local convection mass transfer coefficient, m/s
h_x = local convection heat transfer coefficient, W/m²·K
K = Gladstone–Dale constant, m³/kg
K_{air} = thermal conductivity of air, W/m·K
K_i = Gladstone–Dale constant of the ith component, m³/kg
L = enclosure width in the beam direction
$L_{v\,pixel}$ = pixel vertical length, m
M = molecular weight of substance, g/mole
M_a = molecular weight of substance a, g/mole
M_{af} = amplification factor
N = fringe order
Nu_l = local Nusselt number
n = refractive index
n_0 = refractive index at room temperature
P = pressure, Pa
R = universal gas constant, 8.3143 J/mol·K
Sh_l = local Sherwood number
T = temperature, K
T^* = nondimensional temperature
x = location, m
Y = fringe thickness
y = fringes spacing or location, m
y^* = nondimensional location
λ = wavelength
ρ = density of mixture, kg/m³
ρ_i = density of the ith component, kg/m³

Subscripts
a = air phase or substance a
b = substance b
w = water vapor
0 = undisturbed state
1 = disturbed state

Introduction

ABSORPTION-TYPE liquid desiccant cooling systems can be activated using a low-temperature heat source. In recent years, due to the adverse environmental effects of CFC refrigerants, considerable research and development activities in the area of solar or heat-assisted open-cycle absorption air-conditioning systems have been conducted.[1–4]

Open-cycle absorption cooling systems require a working fluid that is a binary mixture of an absorbent and a refrigerant. The absorbent may vary in composition from system to system. However, the refrigerant is always water, and it is continually fed to the system from an external source. Some possible absorbents include lithium chloride (LiCl), lithium bromide (LiBr), and calcium chloride ($CaCl_2$), where each of them is mixed with water to form an absorbent solution. In their concentrated form, these absorbents have a high affinity for water vapor. The absorbent loses its chemical absorption potential when it absorbs water during the cooling process and regains this potential during the regeneration process. The key to improving the performance of absorption-type systems lies in enhancing mass transfer into the absorbent solution in the absorber and out of the absorbent solution in the regenerator, since the mass diffusivity of the solution is very small as compared to the thermal diffusivity.

It has been known that the addition of small amounts of surface-active materials can reduce the surface tension of a liquid film. The objective of this study was to investigate the distribution of local heat and mass transfer coefficients in a regeneration process at the air–liquid interface and to determine the effect of introducing additives to enhance the heat and mass transfer rates.

The effect of additives was first discovered by Toms[5] where he determined that adding small amounts of a high molecular weight polymer to a Newtonian fluid in turbulent pipe flow resulted in a significant reduction in pressure drop for a given flow rate. Virk et al.[6] demonstrated that the pressure drop of aqueous polymer solutions decreases with increasing polymer concentration up to a certain limit. He pointed out that there is a lower asymptotic limit below which an increase in polymer concentration has no further influence on the value of the friction factor.

Zawacki et al.[7] studied the effect of several different additives in static absorbers. They found that six- to eight-carbon alcohols greatly enhance the absorption rates of water vapor by lithium bromide solutions in static absorbers by inducing convective motion at, or near, the surface. Zawacki et al.[8] investigated the effect of surface-tension-reducing additives

Received Feb. 17, 1994; revision received Feb. 20, 1995; accepted for publication March 15, 1995.

*Research Assistant, Department of Mechanical Engineering, m/c 251, 842 West Taylor Street.

†Professor, Department of Mechanical Engineering, m/c 251, 842 West Taylor Street.

on the absorption of pure water vapor by flowing lithium bromide water solutions for two systems: 1) a thin-film absorber and 2) an open-channel absorber. They found that convective motion occurred in the thin-film system with an additive introduced, which increased absorption rates. The open-channel absorber using an additive showed a high amount of convective motion, with the solution literally climbing the sidewall of the channel.

Evaporation of water into an airstream is a combined heat and mass transfer process. Typically, such processes cannot be easily visualized, therefore, a two-wavelength, fiber-optic, holographic interferometer is used in this study to help gain insight, both qualitatively and quantitatively, into the combined heat and mass transfer processes that occur in film regeneration. The results obtained from the holograms provide detailed information on the local heat and mass transfer coefficients. The main advantage of this optical method is its nonintrusive nature and the fact that information about the whole field can be obtained by evaluating the interferograms.

A 25% concentration lithium chloride solution was used as a dilute liquid desiccant solution because a lithium chloride liquid desiccant solution reaches its dynamic equilibrium of absorbing and releasing moisture at approximately 20–23%.

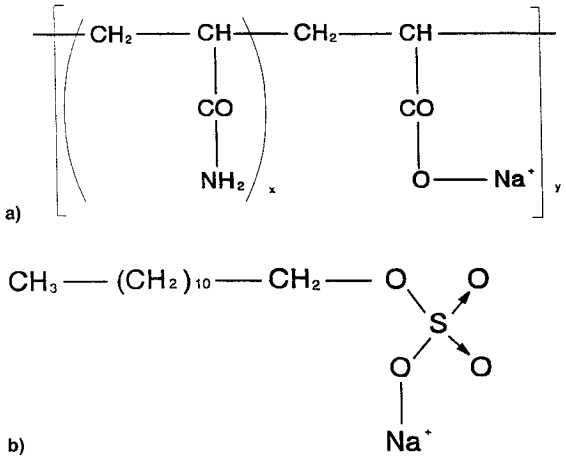

Fig. 1 Chemical structure formula of a) Separan AP-30 and b) SLS.

In industrial systems, a 25–28% lithium chloride concentration is generally defined as a weak desiccant solution.

Wang[9] investigated the influence of additives on nucleate boiling of deionized water. He found that 500-wppm sodium lauryl sulfate with 500-wppm anionic polyacrylamide (Separan AP-30) aqueous solutions enhanced the heat transfer rates in pool boiling at constant heat flux values above 20 W/cm^2. The additives selected in this study were a polymer, a Separan AP-30, and a surfactant, anionic sodium lauryl sulfate (SLS). Both additives are stable chemical compounds. Polyacrylamide, used as a thickening agent and a flocculent, is of high molecular weight and is water-soluble. The average molecular weight of polyacrylamide is between 1×10^4 to 5×10^6. Separan AP-30, chosen for this study, is an anionic polyacrylamide and is linear with a molecular weight of the order of 2,500,000. It may be represented by the generalized structure shown in Fig. 1a. SLS, also named sodium dodecyl sulfate, is an anionic surfactant with a molecular weight 288.38 and is composed of white or cream-colored crystals, or it may be a powder with a faint odor of fatty substances. In industry, SLS is used as a wetting agent and a detergent that is extensively used in the textile industry. Also, it is an ingredient used in many toothpastes. The generalized structure of SLS is shown in Fig. 1b.

Surface active agents are essentially responsible for producing great changes in the surface energy of a liquid or solid. Their ability to cause these changes is associated with their tendency to migrate to the interface between two phases. The effect of these agents on sorption rates is the topic of this study.

Experiment Technique and Apparatus

The experimental setup for investigating the heat and mass transfer at the air/absorbent-film interface, in an inclined channel, is shown schematically in Fig. 2. The system consists of a test chamber, a heating system, an air supply system, and a liquid solution supply system. The test chamber is a rectangular enclosure [20.3 cm (8 in.) × 2.54 cm (1 in.) × 55.6 cm (21.9 in.)], which is supported by a variable-angle steel frame. There are four adjustable screws beneath the test cell to level the test chamber. The sidewalls and the lid of the test chamber are made of 9.5-mm- (3/8-in.-) thick clear Lexan® plastic, and the bottom of the enclosure is made of an 8.0-mm- (5/16-in.-) thick stainless steel plate.

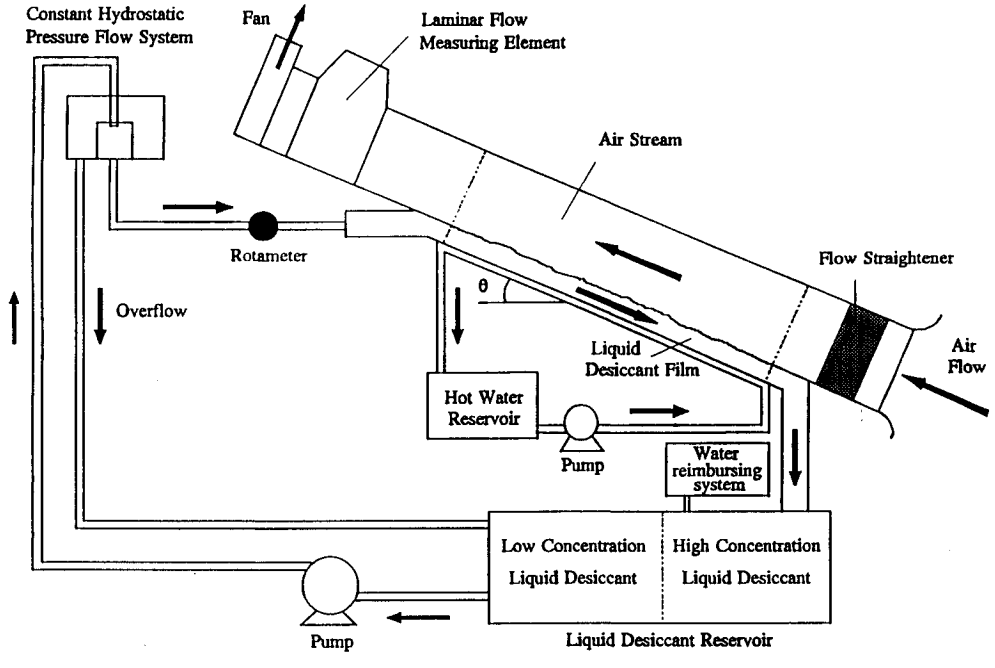

Fig. 2 Schematic diagram of film evaporation test system.

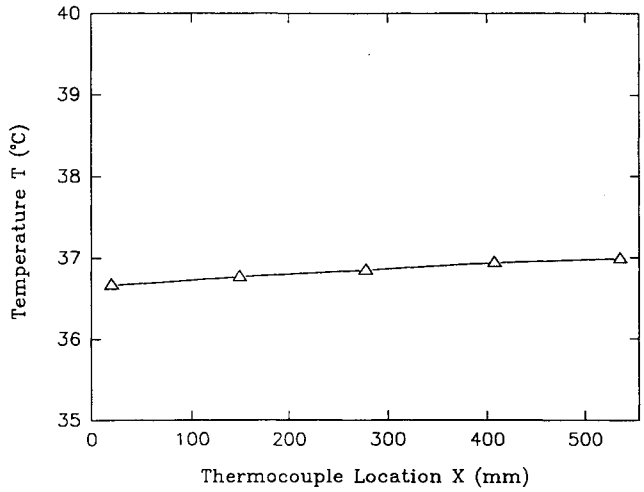

Fig. 3 Temperature distribution along the heating plate.

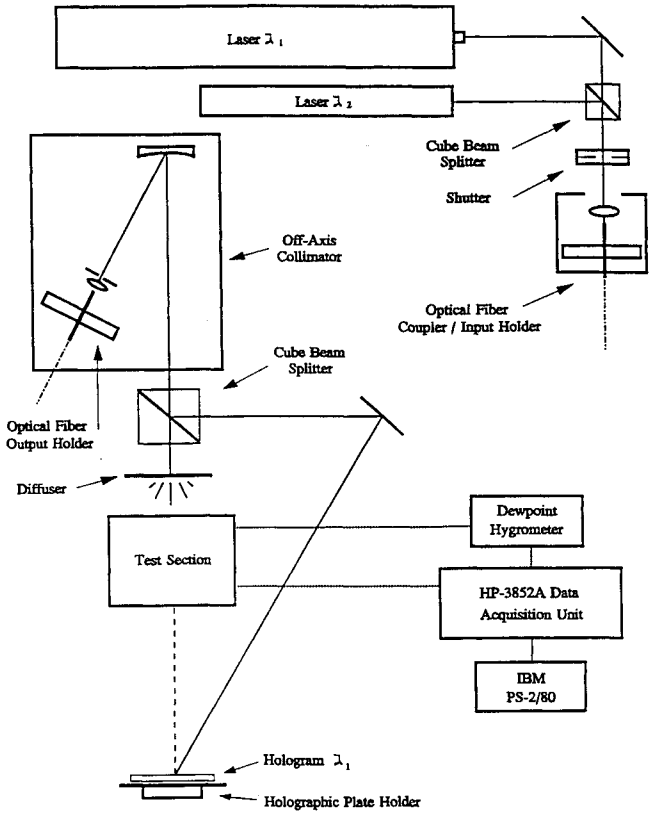

Fig. 4 Schematic of the experiment setup for the fabrication of the holograms.

There are six 1.27-cm- (1/2-in.-) diam copper tubes attached to the bottom of the stainless steel plate through which hot water is passed to heat the test section. The test chamber bottom is insulated to minimize heat losses. There are 39 thermocouples inlaid with a high-thermal-conductivity epoxy at the bottom of the plate to monitor the variation of the plate temperature. To ensure reliable temperature measurements, all of the thermocouples were calibrated in a constant temperature bath, and the uncertainty in the temperature measurements are ±0.1°C. The temperature distribution along the heating plate is shown in Fig. 3 and the temperature across the plate is insured to be uniform by adjusting the heating water flow rates under the plate. A 15.2-cm- (6-in.-) long straight air inlet channel is attached to the test cell to insure that a uniform laminar flow enters the test section. Near the end of the air inlet channel, a small stainless steel tube is inserted into the airflow to aspirate a sample for the dew-point measurement and a thermocouple is used to measure the inlet temperature. The pressure drop across the channel was measured through small pressure taps in the top of the inlet and outlet channel. The outlet channel is identical to the inlet channel.

The holographic interferometric system and the test section, as shown in Fig. 4, were placed on a 121.9 × 182.9 cm (4 × 6 ft) optical table, which was supported by high-pressure, dry air to avoid vibration. The two lasers used in the study were a 5-mW self-contained air-cooled Spectrum Physics He-Ne laser and a 300-mW water-cooled Lexel Argon-ion laser. A computer-based data acquisition system is used for data collection. The system is used for monitoring the experimental system and for collecting data used to determine the overall heat and mass transfer rates.

Optical Data Reduction

The refractive index of a gas is given by the Gladstone–Dale relation,[10] where ρ is gas density. The Gladstone–Dale constant K is a property of the gas, it is

$$n - 1 = K\rho \tag{1}$$

which is a function of wavelength and is nearly independent of temperature and pressure under moderate physical conditions. For a mixture of gases, the Gladstone–Dale constant can be calculated as follows[11]:

$$K = \sum_i a_i K_i \tag{2}$$

where a_i is the mass fraction, and K_i the Gladstone–Dale constant, of the ith component. The mass fraction a_i is defined to be equal to ρ_i/ρ. For an isothermal binary mixture of components a and b, Eqs. (1) and (2) can be combined to give

$$n - 1 = \rho_a K_a + \rho_b K_b \tag{3}$$

In most circumstances, the density of a gas can be calculated using the ideal gas equation of state

$$\rho = MP/RT \tag{4}$$

where P is the pressure, M is the molecular weight of the gas, $R = 8.3143$ J/mol·K is the universal gas constant, and T is the absolute temperature. Combining Eqs. (1–4) yields[10]:

$$\Delta n = n(x, y) - n_0 = \frac{\rho_b}{M_b}(M_b K_b - M_a K_a) + \frac{M_a K_a P}{R}\left(\frac{1}{T} - \frac{1}{T_0}\right) \tag{5}$$

where ρ_b is the mass concentration of substance b, M_a and M_b are the molecular weights of substances a and b, respectively. Equation (5) has two unknowns, T and ρ_b. It is possible to apply two-wavelength interferometry to obtain a second equation to determine the temperature and concentration field of the air, since the Gladstone–Dale constants depend on wavelength. With the help of the holographic interferometer, the local temperature and concentration distributions are determined by evaluating the holograms.

The local Nusselt number at the liquid surface is defined as

$$Nu_l \equiv \frac{h_x D_h}{K_{\text{air}}} = \left.\frac{\partial T^*}{\partial y^*}\right|_{y^*=0} \tag{6}$$

This parameter is equal to the dimensionless temperature gradient at the surface, and it provides a measure of the convection heat transfer occurring at the surface. The local Sherwood number at the liquid surface is defined as

$$Sh_l \equiv \frac{h_{m,x} D_h}{D_{AB}} = \left.\frac{\partial C_A^*}{\partial y^*}\right|_{y^*=0} \tag{7}$$

This parameter is equal to the dimensionless concentration gradient at the surface and it provides a measure of the convection mass transfer occurring at the surface.

Error Analysis

The measuring error includes the fringe thickness measurement error ΔY, and temperature and concentration measurement error ΔT and ΔC_A. The fringe thickness measurement error is inversely proportional to the fringe thickness. In our study, the error was reduced by magnifying the image and using a high-resolution digital imaging processing measurement device. The measurement error is proportional to the resolution of the image processing monitor. In the experiment, the analysis monitor has 512 × 480 pixels, and the measurement error ΔY is proportional to half of the vertical length of one monitor pixel divided by the amplification factor, or

$$\Delta Y \propto (L_{v\text{pixel}}/2M_{af})Y \tag{8}$$

where $L_{v\text{pixel}}$ is the vertical length of one pixel, M_{af} is the amplification factor, and Y is the real dimensional of the measuring object. In this experiment, the fringe spacing error is estimated to be ±2.5%.

The error involved in measuring temperature is estimated to be ±0.5% based on standard thermocouple tables. However, the dew-point temperature measurements are a function of voltage recorded by the data acquisition unit. For dc voltage measurements, Hewlett–Packard specifies a maximum error of 0.008% for the range of interest. This corresponds to an error in dew point of ±0.68°C. Therefore, the relative error involved in measuring concentration in the airstream is estimated to be ±2.5%.

The change in the fringe order caused by diffraction error is given by Hauf and Grigull[13] as

$$\Delta N = n_0 \lambda L/12b^2 \tag{9}$$

For the two-wavelength technique, the fringe thickness in the airfield is different for each wavelength hologram. The ratio of the fringe thickness for the argon hologram to the fringe thickness for the helium–neon hologram has a serious effect on the temperature gradient found from this experiment.

According to Eq. (6), the error in the local Nusselt number measurement in this experiment is given by

$$\Delta Nu_l = \left|\frac{\partial Nu_l}{\partial T}\Delta T\right| + \left|\frac{\partial Nu_l}{\partial C_A}\Delta C_A\right| + \left|\frac{\partial Nu_l}{\partial N}\Delta N\right| + \left|\frac{\partial Nu_l}{\partial Y}\Delta Y\right| \tag{10}$$

A similar procedure was followed for the evaluation of the error in determining the local Sherwood number. The overall total error for the local Nu_l and Sh_l was ±5%.

Experimental Results

All the local temperature and concentration measurements in the airstream in the enclosure were performed using a double-wavelength holographic interferometer. Experiments were conducted for a fixed air and film flow rate, and the Reynolds numbers for the air and film were 1350 and 130,

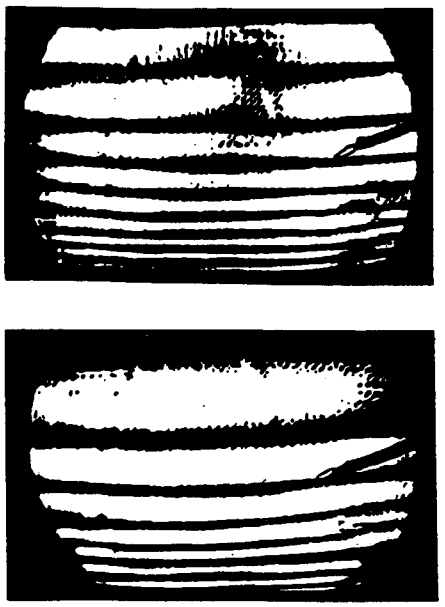

Fig. 5 Holographic interferograms at the air outlet without rods for a 25% by weight LiCl solution constructed by a) 514.5 and b) 632.8 nm.

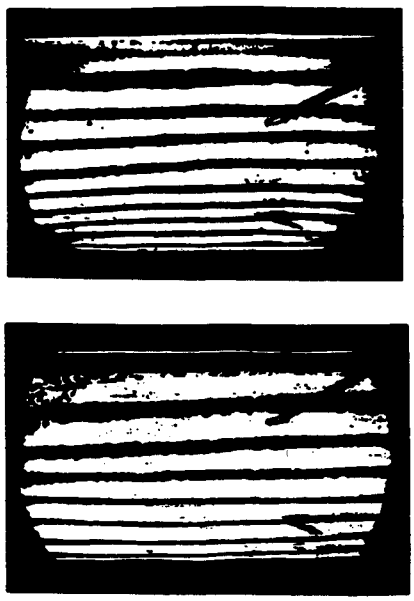

Fig. 6 Holographic interferograms at the air outlet without rods for LiCl–SLS solution constructed by a) 514.5 and b) 632.8 nm.

respectively. The airstream and liquid-film temperature at the inlet and outlet of the test section were measured using thermocouples, and the water–vapor concentration at the inlet and outlet was measured using a General Eastern optical dew-point hygrometer.

Figure 5 shows two typical holograms that are used to determine the temperature and concentration distributions in the air at the exit of channel for the case of a 25% lithium chloride solution film with no additives. This is compared to Fig. 6, which shows two holograms that are used to determine the temperature and concentration distributions in the air at the exit of channel for the case of a 25% lithium chloride solution having a 500-wppm SLS concentration. Also, Fig. 5 is compared to Fig. 7, which shows the two holograms taken with wavelengths of 514.5 and 632.8 nm in the air at the exit of the channel for the case of 25% lithium chloride with a

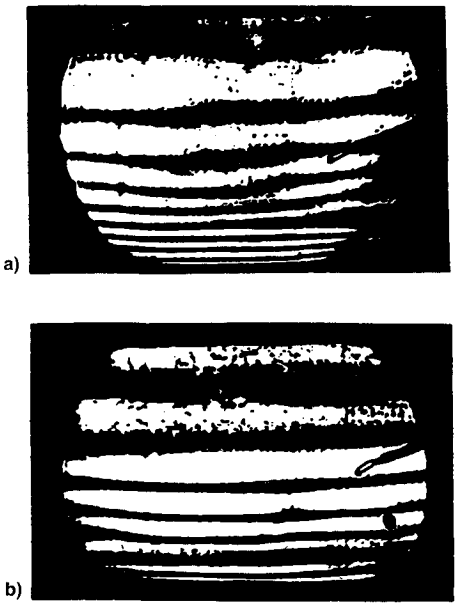

Fig. 7 Holographic interferograms at the air outlet without rods for LiCl–Separan AP-30 solution constructed by a) 514.5 and b) 632.8 nm.

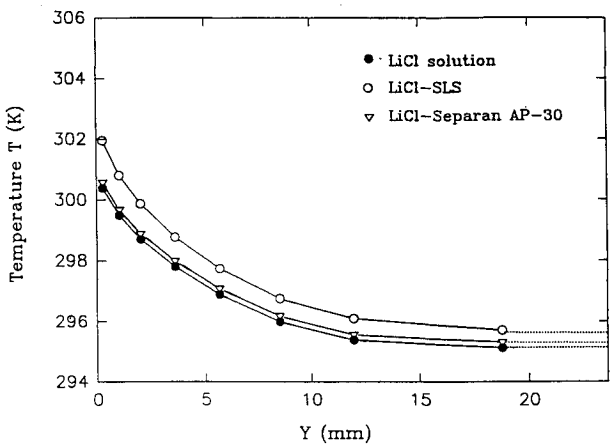

Fig. 8 Temperature distribution at air outlet with different solutions.

500-wppm Separan AP-30 concentration. All of these holograms demonstrate a similar trend that the fringes at the solution surface are thinner and more condensed, which indicates that the temperature and concentration gradients are larger near the solution surface. The fringes are parallel, which illustrates the airflow is in the fully developed laminar flow region. Also, the fringe spacing in the case of LiCl–SLS solution is more condensed than the other two cases, which shows that the temperature and concentration gradient in the airstream are steeper in the LiCl–SLS solution case, which indicates higher heat and mass transfer rates. The holograms were processed using image-processing software, and the fringe grayness is plotted along the vertical direction from each hologram. The fringe grayness data were smoothed by the Savinsky–Golay method[12] and the fringe peaks are distinct and easy to locate.

Since SLS and Separan AP-30 are stable chemical compounds, we assume that the addition of 500-wppm SLS and Separan AP-30 does not change the properties of the lithium chloride solution.[9] With the knowledge of the temperature and concentration at the reference point in the test system, which was located at the thermocouple position, the temperature and concentration distributions in the airfield at the

Table 1 Local Nusselt and Sherwood numbers for Air–H_2O mixture with different solutions at the channel exit

Fluid	Nu_l	Sh_l	h_l, W/m^2·K	$h_{m,l}$, m/s
LiCl solution	5.27	4.94	33.9	0.031
LiCl–SLS	6.32	5.93	41.3	0.040
LiCl–Separan AP-30	5.28	4.94	33.9	0.031

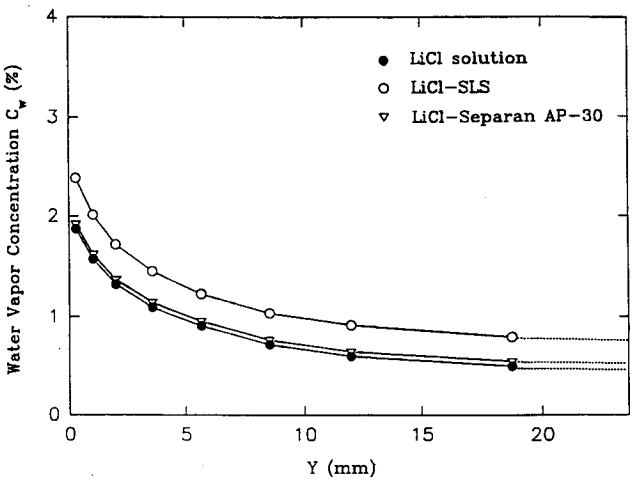

Fig. 9 Concentration distribution at air outlet with different solutions.

channel exit with and without additives were calculated using the two holograms. The results calculated from Eq. (5) are shown in Figs. 8 and 9. The Nusselt and Sherwood numbers at the interface were obtained by differentiating the curve-fitted equations of the temperature and concentration distributions with respect to y^* and evaluating the gradient at $y^* = 0$. The results are tabulated in Table 1.

Comparing the Nusselt and Sherwood between pure LiCl solution and LiCl–SLS solution, the experimental values of the Nusselt and Sherwood numbers for LiCl–SLS solution are higher than the values found in the case of pure LiCl solution. The heat transfer coefficient increases 20% and the mass transfer coefficient increases 30% in the LiCl–SLS solution case. It is believed that the surfactant SLS serves as a surface tension reducing agent that migrates to the interface between the air and liquid phases, reducing the lithium chloride surface tension and causing higher mass transfer rates. Due to the surface tension reduction, the Nusselt and Sherwood numbers with LiCl–SLS solution are higher compared to the pure LiCl solution case.

It is observed that the presence of the 500-wppm Separan AP-30 did not affect the heat and mass transfer performance of the lithium chloride solution. However, the presence of polymer Separan AP-30 in LiCl solution reduces the pressure drop for a given liquid desiccant solution flow rate. In fact, for a condition investigated in this study (i.e., 500-wppm Separan AP-30), a 16% reduction in pumping power occurred. Therefore, the addition of Separan would significantly reduce the pumping power in absorption systems.

Conclusions

It is found that the heat and mass transfer rates in liquid desiccant regeneration can be improved by adding small amounts of surfactant. The selected surfactant, sodium lauryl sulfate, has a strong influence on the surface tension of the LiCl solution. It is believed that the improvement of the heat and mass transfer in film desorption is because the addition of surfactant SLS substantially reduces the surface tension of LiCl solution. In contrast, the presence of polyacrylamide to a LiCl solution does not affect the surface tension of the fluid.

The addition of the polymer Separan AP-30 has no influence on the heat and mass transfer from the LiCl solution. However, since Separan AP-30 lowers the viscosity of the solution, the liquid desiccant pumping power required is reduced by adding 500-wppm Separan AP-30.

References

[1]Factor, H. M., and Grossman, G., "A Packed Bed Dehumidifier/Regenerator for Solar Air Conditioning with Liquid Desiccant," *Solar Energy*, Vol. 24, No. 6, 1980, pp. 541–550.

[2]Löf, G. O. G., Leuz, T. G., and Rao, S., "Coefficients of Heat and Mass Transfer in a Packed Bed Suitable for Solar Regeneration of Aqueous Lithium Chloride Solution," *Journal of Solar Energy Engineering*, Vol. 106, No. 4, 1984, pp. 387–392.

[3]Nelson, D. J., and Wood, B. D., "Evaporation Rate Model for a Natural Convection Glazed Collector/Regenerator," *Journal of Solar Energy Engineering*, Vol. 112, No. 1, 1990, pp. 51–57.

[4]Peng, C. S. P., and Howell, J. R., "The Performance of Various Types of Regenerators for Liquid Desiccants," *Journal of Solar Energy Engineering*, Vol. 106, No. 2, 1984, pp. 133–141.

[5]Toms, B. A., "Some Observations on the Flow of Laminar Polymer Solutions Through Straight Tubes at Large Reynolds Numbers," *Proceeding of the 1st International Congress on Rheology*, Vol. 2, North-Holland, Amsterdam, 1948, pp. 135–141.

[6]Virk, P. S., Mickley, H. S., and Smith, K. A., "The Ultimate Asymptote and Mean Flow Structure in Toms' Phenomenon," *AIChE Journal*, Vol. 37, No. 2, 1970, pp. 488–493.

[7]Zawacki, T., Leipziger, S., and Weil, S. A., "Inducement of Convective Motion in Static Absorbers," Fourth Joint Chemical Engineering Conf. A.I.Ch.E.-C.S.Ch.E., Vancouver, British Columbia, Canada, Sept. 1973.

[8]Zawacki, T., Macriss, R. A., and Rush, W. F., "The Effect of Additives in the Level of Instability of Gas/Liquid Interfaces: The Absorption of Water Vapor by Concentrated Lithium Bromide Solutions in Falling Film and Open Channel Absorbers," 75th National Meeting A.I.Ch.E., Detroit, MI, 1973.

[9]Wang, T. A., "Influence of Surfactants on Nucleate Pool Boiling of Aqueous Polyacrylamide Solutions," Ph.D. Dissertation, Univ. of Illinois, Chicago, IL, 1993.

[10]Vest, C. M., *Holographic Interferometry*, Wiley, New York, 1979.

[11]Merzkirch, W., *Flow Visualization*, Academic, New York, 1974.

[12]Annino, R., and Driver, R., *Scientific and Engineering Applications with Personal Computers*, Wiley, New York, 1986.

[13]Hauf, W., and Grigull, U., "Optical Methods in Heat Transfer," *Advances in Heat Transfer*, Vol. 6, 1970, pp. 133–367.